Structural Study, Mössbauer Spectra and Electrical Properties of $R_5Fe_6Sn_{18}$ (R = Tm, Lu) Compounds

I. Shcherba[a,*], L. Romaka[a], A. Skoblik[b], B. Kuzel[a], H. Noga[c], L. Bekenov[b], Yu. Stadnyk[a], P. Demchenko[a] and A. Horyn[a]

[a]Ivan Franko L'viv National University, Kyryla and Mefodiya Str. 6,8, 79005 L'viv, Ukraine

[b]Institute for Metal Physics, NAS of Ukraine, Vernadskogo Str. 36, 03142 Kyiv, Ukraine

[c]Institute of Technology, Pedagogical University, Podchorążych 2, 30-084 Cracow, Poland

(Received October 26, 2018; revised version February 18, 2019; in final form February 24, 2019)

Ternary intermetallic $R_5Fe_6Sn_{18}$ (R = Tm, Lu) compounds have been synthesized from the elements by arc melting, annealed at 670 K and characterized by X-ray powder diffraction and energy dispersive X-ray analyses. Performed structure refinements have shown that they crystallize in the cubic $Tb_5Rh_6Sn_{18}$ structure type (space group Fm-3m, $a = 13.55399(4)$ Å, $a = 13.53243(5)$ Å for Tm and Lu compounds, respectively). Using ^{57}Fe Mössbauer spectroscopy it has been found that the magnetic state of the Fe atoms in the $Tm_5Fe_6Sn_{18}$ and $Lu_5Fe_6Sn_{18}$ stannides is paramagnetic. The value of the isomer shifts for $Lu_5Fe_6Sn_{18}$ and $Tm_5Fe_6Sn_{18}$ is positive relative to pure Fe. The ^{57}Fe Mössbauer spectra for $Lu_5Fe_6Sn_{18}$ and $Tm_5Fe_6Sn_{18}$ stannides have shown that the quadrupole splitting for the Fe position (24e) have magnitudes of 0.43 and 0.45 mm/s, respectively. The similarity of these values is consistent with a qualitative crystal structure analysis. The examined $Tm_5Fe_6Sn_{18}$ and $Lu_5Fe_6Sn_{18}$ compounds have been found to be characterized by metallic-like conductivity and high values of electrical resistivity (672.9 $\mu\Omega$ cm, 623.8 $\mu\Omega$ cm at 300 K for Tm and Lu, respectively).

DOI: 10.12693/APhysPolA.136.158

PACS/topics: intermetallics, quadrupole splitting, Mössbauer spectra, electrical resistivity

1. Introduction

The series of RM_xSn_y intermetallics (R = rare earth element, M = Co, Ru, Rh, Os, Ir) is characterized by several types of the crystal structures indicated as phases I, II, III, V, and VII [1–3]. The RM_xSn_y compounds were analyzed in detail and discussed by Skolozdra in Ref. [4]. These compounds are interesting because some of them show superconductivity and magnetic ordering. The main feature of these phases is a mixture of rare earth and tin atoms in one of the crystallographic positions, and the presence of the metallic and covalent bonding. The phase I of stannides with the formula $R_6M_8Sn_{26}$ has a simple cubic structure (space group Pm-3m) with the lattice parameter $a = 0.97$ nm. In Ref. [5] the authors described the structure of the phase I ($Yb_3Rh_4Sn_{13}$-type) as a three-dimensional array of corner-sharing trigonal prisms with Rh atoms in the centers. The phase III according to X-ray data has a cubic structure (space group F-43m, $a = 1.37$ nm) with the formula $Tb_5Rh_6Sn_{18}$ [6]. For stannides with the formula $SnR_4M_6Sn_{18}$ two structure types were found corresponding to phases II and II′. The structure of the phase II is tetragonal (space group $I4_1/acd$) while the phase II′ has a cubic structure with the space group Fm-3m. X-ray and electron diffraction investigations of the $TbRh_xSn_y$ and $DyOs_xSn_y$ single crystals showed that they can be considered as a disordered microtwinned phase II and these compounds were named as II′ phases (space group Fm-3m) [7]. The structure disordering of the $Tb_5Rh_6Sn_{18}$ stannide concerned the Tb(2) and Sn(2) sublattices of the formula $[Sn(1)_{1-x}Tb_x]Tb(2)_4Rh_6Sn(2)_4Sn(3)_{12}Sn(4)_2$ [7]. In the $Tb_4(Tb_{0.6}Sn_{0.4})Rh_6Sn_{18}$-type a statistical occupation of the 4a sites by terbium and tin atoms was observed [7]. The magnetic and electrical properties of the RM_xSn_y stannides were studied for determination of the superconducting behavior [1–3, 8, 9]. The relation between the crystal structure and superconducting properties of the $[Sn_{1-x}Er_x]Er_4Rh_6Sn_{18}$ phase was analyzed in Ref. [9], where the influence of the variation in (Sn, Er) occupation of the $[Sn_{1-x}Er_x]Er_4$ sublattice upon low temperature properties was observed. The investigation of the R–Ni–Sn ternary systems in the region of high tin concentrations resulted in the discovery of $R_{5-x}Ni_{12}Sn_{24+x}$ cubic phases with a $GdNi_{2.67}Sn_{5.44}$ type structure [10]. The similar occupation of the crystallographic 2a position by a mixture of R and Sn atoms was observed for these phases, and a crystal structure analysis showed slightly different compositions for the representatives of this structure type varied from $R_4Ni_{12}Sn_{25}$ (for Dy) to $R_5Ni_{12}Sn_{48}$ (for La) [10, 11].

In this paper the synthesis and the results of crystal structure, ^{57}Fe Mössbauer spectroscopy, and electrical properties studies of the new $Tm_5Fe_6Sn_{18}$ and $Lu_5Fe_6Sn_{18}$ compounds are reported.

*corresponding author; e-mail: ishcherba@gmail.com

2. Experimental details

Samples with the nominal composition $R_{15}Fe_{20}Sn_{65}$ (R = Tm, and Lu) were prepared using an electric arc furnace by direct arc melting of the constituent elements (overall purity: R — 99.9 wt%, Fe — 99.99 wt%, Sn — 99.999 wt%) in a protective argon atmosphere. The alloys were subsequently annealed at 670 K for 720 h and then cold water quenched. The compositions of the obtained samples were examined by scanning electron microscopy (SEM) using the scanning electron microscope REMMA-102-02. A quantitative electron probe microanalysis (EPMA) of the phases was carried out using an energy-dispersive X-ray analyzer with pure elements as standards (acceleration voltage was 20 kV; K- and L-lines were used).

X-ray powder diffraction (XRPD) data were collected in the transmission mode on a STOE STADI P diffractometer (linear PSD detector, $2\theta/\omega$-scan; Cu K_{α_1} radiation, curved germanium (1 1 1) monochromator). The crystal structures were refined by the Rietveld method [12] with the FullProf.2k program (version 4.80) [13] from the WinPLOTR program package [14] applying a pseudo-Voigt profile function and isotropic approximation for the atomic displacement parameters.

The Mössbauer spectra were recorded in the transmission mode. A WISSEL Mössbauer spectrometer and a source of ^{57}Co gamma-quanta in a Cr matrix were used for measurements. The equipment was characterized by the line-width of 0.22 mm/s for the gamma-quanta source. The calibration of isomeric shift values was carried out relative to α-Fe at room temperature.

The electrical resistivity was measured on millimeter-scale, with well-shaped pieces cut by spark erosion from the polycrystalline samples by the standard two-probe technique in the temperature range 10.5–300 K using a helium cooler with a reserved cycle (Advanced Research Systems, USA). The temperature dependence of the magnetic susceptibility was measured by the Faraday method in the 78–300 K temperature range and under a magnetic field up to 0.8 T.

3. Results and discussion

The analysis of the positions of diffraction peaks and their intensities of the $Tm_{15}Fe_{20}Sn_{65}$ and $Lu_{15}Fe_{20}Sn_{65}$ samples led to a cubic structure of the $Tb_4(Tb_{0.6}Sn_{0.4})Rh_6Sn_{18}$-type [7] (the so-called phase II′, space group $Fm\text{-}3m$). The experimental conditions of the structure refinements and crystallographic

TABLE I

Experimental details and crystallographic data for $R_5Fe_6Sn_{18}$ (R = Tm, Lu) compounds

Formula	$Tm_5Fe_6Sn_{18}$	$Lu_5Fe_6Sn_{18}$
space group – Wyckoff sequence / Pearson symbol	$Fm\text{-}3m$ (No. 225) – kf^2eca / $cF196-80$	
structure type	$Tb_4(Tb_{0.6}Sn_{0.4})Rh_6Sn_{18}$	
Mr / Z	3316.52 / 4	3346.68 / 4
lattice parameter a [Å]	13.55399(4)	13.53243(5)
cell volume V [Å^3]	2490.013(11)	2478.151(15)
calculated density D_x [g/cm^3]	8.846	8.969
absorption coefficient μ (Cu K_α) [mm^{-1}]	199.10	204.65
specimen shape / particle morphology / colour	Flat sheet ($8\times8\times0.1$ mm) / loose powder, grain size $<$ 0.04 mm / light-grey	
data collection temperature T [K]	297(1)	
diffractometer	STOE STADI P (Transmission mode)	
radiation, wavelength λ [Å]	Cu K_{α_1}, 1.540598	
angular range for data collection / increment 2θ [°]	$6.000 \le 2\theta \le 110.045$ / 0.015	$6.000 \le 2\theta \le 110.045$ / 0.015
linear PSD step 2θ [°] / time [s/step]	0.480 / 375	0.480 / 375
number of measured reflections	115	115
number of refined parameters	19	19
reliability factors:		
$R_I = \Sigma\lvert I_{obs} - I_{calc}\rvert/\Sigma\lvert I_{obs}\rvert$	0.0245	0.0154
$R_F = \Sigma\lvert F_{obs} - F_{calc}\rvert/\Sigma\lvert F_{obs}\rvert$	0.0264	0.0209
$R_p = \Sigma\lvert y_i - y_{c,i}\rvert/\Sigma y_i$	0.0303	0.0340
$R_{wp} = [\Sigma w_i\lvert y_i - y_{c,i}\rvert^2/\Sigma w_i y_i^2]^{1/2}$	0.0385	0.0443
$R_{exp} = [n-p/\Sigma w_i y_i^2]^{1/2}$	0.0371	0.0440
$\chi^2 = \{R_{wp}/R_{exp}\}^2$	1.08	1.02
content of $R_5Fe_6Sn_{18}$ / $FeSn_2$ / Sn phases [wt%]	91.5(4) / 6.7(1) / 1.8(1)	93.2(4) / 4.1(1) / 2.7(1)

data for the $Tm_{15}Fe_{20}Sn_{65}$ and $Lu_{15}Fe_{20}Sn_{65}$ samples are summarized in Table I. Other types of the related structures, i.e., the so-called phase II (tetragonal $Er_4(Er_{0.33}Sn_{0.67})Rh_6Sn_{18}$-type, space group $I4_1/acd$ [15]) and phase III (cubic $Tb_5Rh_6Sn_{17}$-type, space group F-43m [5]) according to the classification of Ref. [1], were tested and rejected. The final atomic and isotropic displacement parameters for both compounds are given in Table II.

TABLE II

Fractional atomic coordinates, equivalent isotropic displacement parameters B_{iso} [Å^2] and site occupancies G

Site	R	Wyckoff position	x	y	z	B_{iso} [Å^2]	G
Fe	Tm	24e	0.2554(3)	0	0	0.43(6)	1
	Lu		0.2550(4)	0	0	0.34(7)	
R1	Tm	4a	0	0	0	1.22(7)	1
	Lu					0.97(7)	
R2	Tm	32f	0.3672(7)	0.3672(7)	0.3672(7)	1.07(5)	0.5
	Lu		0.3668(5)	0.3668(5)	0.3668(5)	0.60(5)	
Sn1	Tm	32f	0.4097(1)	0.4097(1)	0.4097(1)	1.11(9)	0.5
	Lu		0.4097(1)	0.4097(1)	0.4097(1)	0.59(9)	
Sn2	Tm	96k	0.1722(9)	0.1722(9)	0.0084(4)	0.51(4)	0.5
	Lu		0.1729(2)	0.1729(2)	0.0083(5)	0.53(5)	
Sn3	Tm	8c	1/4	1/4	1/4	1.71(3)	1
	Lu					1.77(4)	

Recently we have published a report on the crystal structure of the $Er_5Fe_6Sn_{18}$ compound with $Tb_4(Tb_{0.6}Sn_{0.4})Rh_6Sn_{18}$-type [16]. The full occupation of the 4a position was established exclusively by Er atoms in contrast to the parent $Tb_4(Tb_{0.6}Sn_{0.4})Rh_6Sn_{18}$-type [7], where a statistical occupation of the 4a site by terbium and tin atoms was observed. A similar phenomenon is observed in the $Tm_5Fe_6Sn_{18}$ and $Lu_5Fe_6Sn_{18}$ compounds at 670 K: the Tm and Lu atoms fully occupied the 4a site corresponding to formula $R_5Fe_6Sn_{18}$. The obtained compositions of the both phases are in good agreement with the EPMA data ($Tm_{17.76}Fe_{19.63}Sn_{62.61}$ and $Lu_{17.56}Fe_{19.63}Sn_{62.81}$). Also, attention is drawn to the similarity of the values of atomic displacement parameters in the investigated structures and in the $Tb_4(Tb_{0.6}Sn_{0.4})Rh_6Sn_{18}$ structure, i.e. small values are observed for Fe(Rh) atoms and the largest values are observed for Sn atoms in a tetrahedral coordination Sn[R_4] (8c site). The model of the $Lu_5Fe_6Sn_{18}$ structure and the stacking of coordination polyhedra are shown in Fig. 1.

The analysis of the interatomic distances (Table III) showed that the distances between Fe–Sn2, Fe–Sn1, Sn1–Sn1, and R2–Sn3 atoms are shorter than the sum of the respective atomic radii, which is probably caused by partial occupation of the crystallographic positions for R2, Sn1, and Sn2 atoms and a contribution of the covalence into the bond. The based $Tb_5Rh_6Sn_{18}$ structure is characterized by analogous shortening of interatomic distances between Rh–Sn and Tb–Sn atoms.

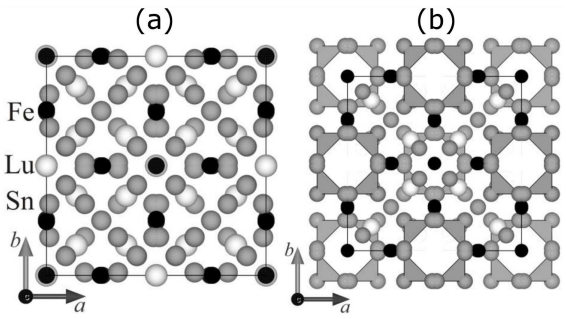

Fig. 1. Model of the $Lu_5Fe_6Sn_{18}$ structure (a) and stacking of cuboctahedrons in $Lu_5Fe_6Sn_{18}$ structure (b).

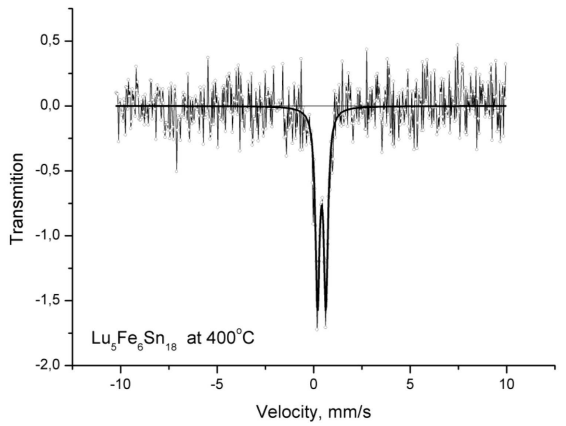

Fig. 2. Mössbauer spectrum of the $Lu_5Fe_6Sn_{18}$ stannide at room temperature.

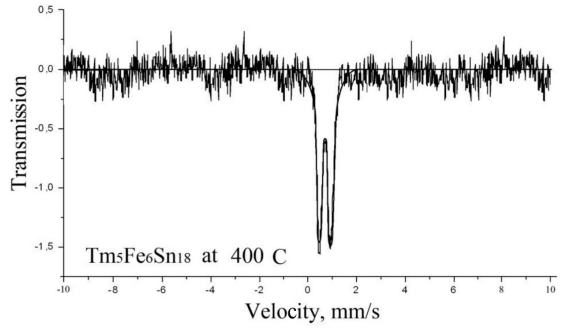

Fig. 3. Mössbauer spectrum of the $Tm_5Fe_6Sn_{18}$ stannide at room temperature.

TABLE III

Main interatomic distances in the $R_5Fe_6Sn_{18}$ (R = Tm, Lu) compounds [nm]

Atom	Tm	Lu
Fe–Sn2	0.2595	0.2593
Fe–Sn1	0.2715	0.2715
Fe–R2	0.2962	0.2964
R1–Sn2	0.3304	0.3311
R2–Sn3	0.2753	0.2739
R2–Sn1	0.3130	0.3133
R2–Sn2	0.3180	0.3167
Sn1–Sn1	0.2448	0.2444

To study the magnetic state of iron atoms in the $Tm_5Fe_6Sn_{18}$ and $Lu_5Fe_6Sn_{18}$ compounds we used ^{57}Fe Mössbauer spectroscopy. The corresponding Mössbauer spectra obtained for the $Lu_5Fe_6Sn_{18}$ and $Tm_5Fe_6Sn_{18}$ compounds are shown in Figs. 2, 3, and their parameters are presented in Table IV.

TABLE IV

Essential Mössbauer spectroscopy parameters for the $Lu_5Fe_6Sn_{18}$ and $Tm_5Fe_6Sn_{18}$ compounds at room temperature

Compound	A [%]	IS [mm/s]	QS [mm/s]	G [mm/s]
$Lu_5Fe_6Sn_{18}$	100	0.41 ± 0.02	0.43 ± 0.02	0.26
$Tm_5Fe_6Sn_{18}$	100	0.44 ± 0.02	0.46 ± 0.02	0.27

In the absence of an external magnetic field there is no magnetic splitting in the spectrum of $Lu_5Fe_6Sn_{18}$ and $Tm_5Fe_6Sn_{18}$, indicating either the absence of a magnetic moment at the Fe site or spin relaxation, and then $\nu_s \gg \nu_{hf}$. To clarify the situation the sample should be exposed to an external magnetic field H_{ext}.

Here A (%) is the contribution of the respective subprofile to the total absorption profile, and the Mössbauer spectroscopy parameters are: the isomer (total) shift versus α-Fe [IS (mm/s)], quadrupole splitting [QS (mm/s)], absorber line-width [G (mm/s)].

The value of the isomer shift (IS) for $Lu_5Fe_6Sn_{18}$ and $Tm_5Fe_6Sn_{18}$ compounds is positive and slightly higher than measured chemical shifts in the studied RFe_6Sn_6 stannides (R = Tm, Yb, Lu) [17, 18] or other intermetallic compounds containing iron [19, 20], for example in the Sc–Fe–Si systems, in which no magnetic moment was observed at Fe sites in the ternary compounds [19]. Those compounds have a small positive isomer shift relative to pure Fe. The shift sign indicates that the electronic density at Fe nuclei in those ternary compounds is less than that at the radiating Fe nuclei. It is well known that an increase in the number of d-electrons leads to a decrease in the density of s-electrons at the nucleus and indirectly results in a positive isomer shift. Of course, the importance of the contribution of the density of p-electrons to the value of the isomer shift should be noted, since similar to 3d-electrons, 4p-electrons shield s-electrons from the nucleus and indirectly determine the positive isomer shift. However, the screening effect of 4p-electrons is approximately 1.5 times weaker than the 3d-electron shielding effect. The absence of a local magnetic moment at the Fe atoms is confirmed by the absence of a magnetically split component in the Mössbauer spectrum. The values of the isomer shift and quadrupole splitting parameters indicate the paramagnetic nature of the magnetic interaction.

An extremely important parameter of the Mössbauer spectrum is the quadrupole splitting (QS). It characterizes the interaction of the electric quadrupole moments of the nuclei with internal crystal electric fields. The quadrupole moment of the nucleus θ reflects the degree of deviation of its shape from the spherical one.

As can be seen from the crystal structure cell (Fig. 1) the coordination number of the Fe atom is 12, and the coordination polyhedron is a slightly deformed cuboctahedron which is formed by 4Sn1 atoms (2.715 Å) and 8Sn2 atoms (2.593 Å).The ^{57}Fe Mössbauer spectra for $Lu_5Fe_6Sn_{18}$ and $Tm_5Fe_6Sn_{18}$ show that the quadrupole splitting for the Fe position (24e) have magnitudes of 0.43 and 0.45 mm/s, respectively. The similarity of these values is consistent with the above qualitative crystal structure analysis, which revealed that the Fe nearest neighbors are exclusively tin atoms (Fig. 1b), and the electric field gradient is determined for the most part by the tin atoms that are located at the vertices of the cuboctahedron and have reduced Fe–Sn distances.

Because of a strong covalent interaction between Fe and Sn atoms that surround them the increase in the population of d-states is due to the valence Sn electrons, and the number of Fe s-electrons is almost unchanged.

The measurements of the magnetic susceptibility of the $Lu_5Fe_6Sn_{18}$ compound confirmed its paramagnetic state. Studied compound is characterized by small values of the magnetic susceptibility with values $\chi = 25.42 \times 10^{-6}$ cm^3/g at 78 K and $\chi = 21.91 \times 10^{-6}$ cm^3/g at 300 K. The analysis of the temperature dependence of the inverse magnetic susceptibility indicated that $\chi^{-1}(T)$ behavior does not correspond to a modified Curie–Weiss law.

The examined $Tm_5Fe_6Sn_{18}$ and $Lu_5Fe_6Sn_{18}$ compounds are characterized by metallic-like conductivity in the temperature range from 10.5 K to 300 K and a large deviation from linearity of the temperature dependence of resistivity at high temperatures (Fig. 4). At low temperatures under cooling the resistivity predictably tends to a constant value (residual resistivity). As evident from Fig. 4, change of the resistivity caused by magnetic ordering was not observed on the $\rho(T)$ dependence for the $Tm_5Fe_6Sn_{18}$ compound up to 11 K. The temperature dependence parameters are presented in Table V. The absolute values of the resistivity of the $Tm_5Fe_6Sn_{18}$ and $Lu_5Fe_6Sn_{18}$ stannides are much higher (672.9 $\mu\Omega$ cm, 623.8 $\mu\Omega$ cm at 300 K for Tm and Lu, respectively) than for the most intermetallics (Table V). As reported in the literature [1–4] most of the RM_xSn_y phases have a high resistivity values and authors concluded that one of the causes of high resistivity values is the presence of a significant ion-covalent contribution to the bonding.

TABLE V

Parameters of the temperature dependence of the electrical resistivity of $Lu_5Fe_6Sn_{18}$ and $Tm_5Fe_6Sn_{18}$.

Compound	$\rho_{290\text{K}}$ [$\mu\Omega$ cm]	$\rho_{10.5\text{K}}$ [$\mu\Omega$ cm]	$\rho_{290\text{K}}/\rho_{10.5\text{K}}$	$(\rho_{\text{exp}} - \rho_{\text{linear}})/\rho_{\text{linear}}$ [%]
$Tm_5Fe_6Sn_{18}$	672	154	4.3	19.1
$Lu_5Fe_6Sn_{18}$	620	482	1.3	4.2

ρ_{exp} is the experimental resistivity value at 150 K and ρ_{linear} is the resistivity value at 150 K in the case of imaginary linear temperature dependence.

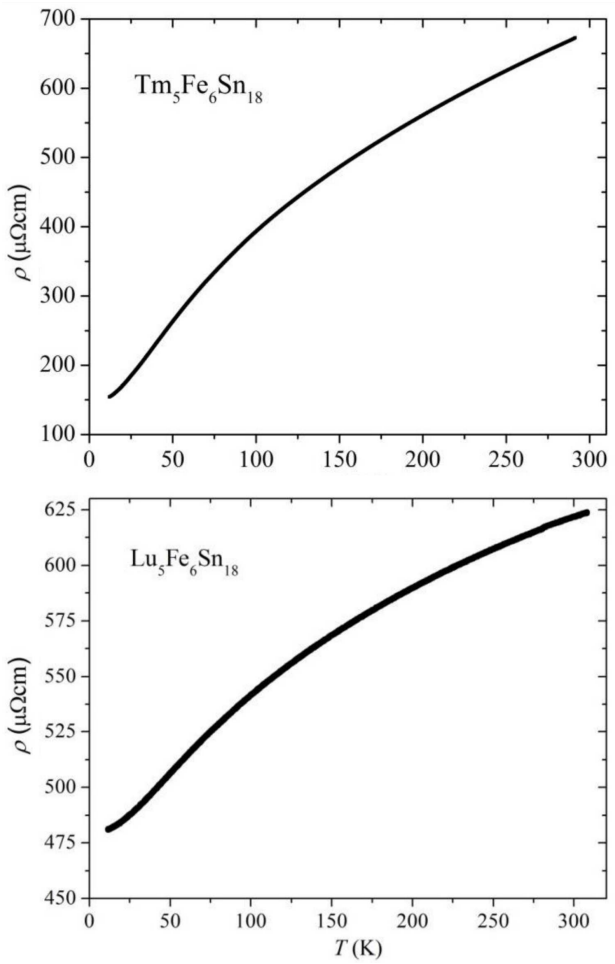

Fig. 4. The temperature dependence of the electrical resistivity of the $Tm_5Fe_6Sn_{18}$ and $Lu_5Fe_6Sn_{18}$.

The observed character of the temperature dependence of electrical resistivity was discovered for the first time in actinides and was classified as anomalous [21, 22]. Then such the character of the temperature dependence of electrical resistivity was observed in many intermetallic compounds, such as YCo_2, Y_4Co_3, $Y_6(Fe,Mn)_{23}$, $Er_6(Fe,Mn)_{23}$ [23] and also for related series of the $R_{5-x}Ni_{12}Sn_{24+x}$ cubic phases with $GdNi_{2.67}Sn_{5.44}$ type structure [10]. One of the conditions for this type of the temperature dependence is the presence of a transition element in the compound, particularly a 3*d*-element.

Resistivity of a real sample can be written (taking into account the Matthissen rule) as

$$\rho(T) = \rho_0 + \rho_{ph}(T) + \rho_{mag}(T),$$

where ρ_0 is the residual resistance, $\rho_{\rm ph}(T)$ is the resistivity caused by the electron–phonon interaction, and $\rho_{\rm mag}(T)$ is an additional component that contains various contributions from different physical mechanisms, such as Mott-type interband scattering, magnetic scattering (including scattering caused by the spin disordering in the presence of disordered magnetic moments) and other possible scattering mechanisms.

As noted above, the temperature dependences of the electrical resistivity of both $Tm_5Fe_6Sn_{18}$ and $Lu_5Fe_6Sn_{18}$ deviate from linearity. At high temperatures the observed decrease of the growth rate of resistivity cannot be correctly approximated by the Bloch–Grüneisen–Mott formula [24] within the studied temperature range. The Bloch–Grüneisen–Mott formula, which takes into account the Mott-type type interband scattering, describes experimental curves well in the case of slight nonlinearity. The greater deviation from the linearity narrows the temperature range within which the approximation is applicable. An approximation in a limited range loses the physical meaning to some extent if the approximation is based on an expression with the physical meaning behind it, as in the case of the Bloch–Grüneisen–Mott formula. Nevertheless (taking into account above remarks), we present the mentioned approximation for $Lu_5Fe_6Sn_{18}$ in Fig. 5 and provide some of its parameters.

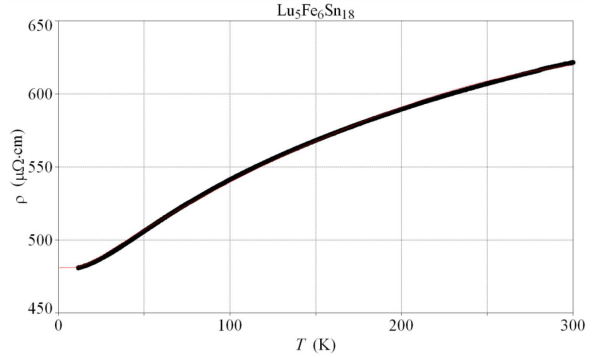

Fig. 5. The approximation of the temperature dependence of the electrical resistivity of $Lu_5Fe_6Sn_{18}$ by the Bloch–Grüneisen–Mott formula in the temperature range 0–225 K ($K_0 \approx \rho_0 = 481$ $\mu\Omega$ cm, $K_2 \approx \Theta_{\rm D} = 107$ K).

Since the approximation by the Bloch–Grüneisen–Mott formula is impossible within the whole temperature range we can conclude that in our case the contribution of the transition metal to the total resistivity is not limited to the contribution to the residual resistivity, phonon component of scattering and Mott's contribution, and $C_{\rm mag}(T)$ has more constituents and determines complex nature of the temperature dependence of the resistivity of $Lu_5Fe_6Sn_{18}$.

In general, the character of the temperature dependences of the electrical resistivity of intermetallic compounds of such type depends on the constituents of a compound (whether it contains a magnetic or nonmagnetic rare-earth element, a magnetic or nonmagnetic transition element), magnetic ordering, and crystal structure. The *d*- and *f*-shells are influenced strongly by the interaction of surrounding ions, which can radically change the magnetic state of the ions.

In addition, the mentioned factors determine a relatively large absolute value of the resistivity of the $Lu_5Fe_6Sn_{18}$ compound. As for the tendency of the

growth rate of resistivity to decrease in the region of "high" temperatures with a temperature increase, one can recall the rule of Mooijh [25], who suggested that if the average free path of conduction electrons decreases to the value of interatomic distances, then the resistivity shows a tendency to become temperature-independent.

4. Conclusion

In our work, crystal structure study of the new $Tm_5Fe_6Sn_{18}$ and $Lu_5Fe_6Sn_{18}$ stannides showed that both compounds crystallize in the cubic $Tb_5Rh_6Sn_{18}$ structure type (space group Fm-$3m$) and enlarge the series of RM_xSn_y intermetallics. The full occupancy of the $4a$ position by Tm and Lu atoms was established which corresponds to formula $R_5Fe_6Sn_{18}$. Comparison of the shortening of interatomic distances between Fe–Sn and R–Sn atoms with $Tb_4(Tb_{0.6}Sn_{0.4})Rh_6Sn_{18}$ parent type was made.

The magnetic state of the Fe ion in $Lu_5Fe_6Sn_{18}$ and $Tm_5Fe_6Sn_{18}$ has been examined by ^{57}Fe Mössbauer spectroscopy and it has been found to be paramagnetic. The values of the isomer shift for $Lu_5Fe_6Sn_{18}$ and $Tb_5Fe_6Sn_{18}$ have been found to be positive. The shift sign indicates that the electronic density at Fe nuclei in these compounds is less than that at the radiating nuclei of pure Fe. The ^{57}Fe Mössbauer spectra for $Lu_5Fe_6Sn_{18}$ and $Tm_5Fe_6Sn_{18}$ showed that the quadrupole splitting for the Fe position ($24e$) have a value of 0.43–0.45 mm/s. The similarity of these values is consistent with a qualitative crystal structure analysis, which revealed that the Fe nearest neighbors are exclusively tin atoms, and the electric field gradient is determined for the most part by the tin atoms that are located at the vertices of the Fe coordination cuboctahedron and have reduced Fe–Sn distances. From both diffraction and Mössbauer data, the crystallographic data indicates the presence only one Fe site (24e) in the structure of the $Tm_5Fe_6Sn_{18}$ and $Lu_5Fe_6Sn_{18}$ compounds. Electrical property measurements showed that the $Tm_5Fe_6Sn_{18}$ and $Lu_5Fe_6Sn_{18}$ compounds are characterized by metallic-like type of conductivity with high resistivity values similarly to the most related RM_xSn_y phases.

References

[1] A.S. Cooper, *Mater. Res. Bull.* **15**, 799 (1980).

[2] G.P. Espinosa, A.S. Cooper, H. Barz, *Mater. Res. Bull.* **17**, 963 (1982).

[3] J.L. Hodeau, M. Marezio, J.P. Remeika, C.H. Chen, *Solid State Commun.* **42**, 97 (1982).

[4] R.V. Skolozdra, in: *Handbook on the Physics and Chemistry of Rare-Earths*, Eds. K.A. Gschneidner, Jr., L. Eyring, Vol. 24, North-Holland, Amsterdam 1997, Ch. 164.

[5] J.M. Vadenberg, *Mater. Res. Bull.* **15**, 835 (1980).

[6] J.L. Hodeau, J. Chenavas, M. Marezio, J.P. Remeika, *J. Solid State Commun.* **36**, 839 (1980).

[7] S. Miraglia, J.L. Hodeau, F.D. Bergevin, M. Marezio, G.P. Espinosa, *Acta Crystallogr. B* **43**, 76 (1987).

[8] F. Gastaldo, M. Giovannini, A. Strudom, R.F. Djuomessi, I. Gurlik, M. Reiffers, P. Solokha, A. Saccone, *Acta Phys. Pol. A* **131**, 1006 (2017).

[9] S. Miraglia, J.L. Hodeau, M. Marezio, H.R. Ott, *Ann. Chim. Fr.* **9**, 1011 (1984).

[10] V.V. Romaka, E.K. Hlil, L. Romaka, D. Gignoux, D. Fruchart, A. Horyn, S. Miraglia, *J. Alloys Comp.* **493**, 35 (2010).

[11] V.V. Romaka, R. Gladyshevskii, Y. Gorelenko, *J. Alloys Comp.* **453**, L8 (2008).

[12] *The Rietveld Method*, Ed. R.A. Young, IUCr Monographs of Crystallography, No. 5, International Union of Crystallography, Oxford University Press, 1993.

[13] J. Rodriguez-Carvajal, *Commission on Powder Diffraction (IUCr), Newsletter No. 26*, 2001, p. 12.

[14] T. Roisnel, J. Rodriguez-Carvajal, *Mater. Sci. Forum* **378**, 118 (2001).

[15] J.L. Hodeau, M. Marezio, J.P. Remeika, *Acta Crystallogr. B* **40**, 26 (1984).

[16] L. Romaka, V.V. Romaka, P. Demchenko, R. Serkiz, *J. Alloys Comp.* **507**, 67 (2010).

[17] T. Mazet, B. Malaman, *J. Alloys Comp.* **325**, 67 (2001).

[18] T. Mazet, O. Isnard, B. Malaman, *J. Magn. Magn. Mater.* **241**, 51 (2002).

[19] O. Razumov, I. Shcherba, B. Kotur, A. Kushnir, *Ukr. Phys. J.* **38**, 99 (1993).

[20] I. Shcherba, Y. Gorelenko, Ya. Dutchak, M. Ristic, *J. Less-Common Met.* **123**, 85 (1986).

[21] G.T. Meadem, *Contemp. Phys.* **12**, 313 (1971).

[22] D.W. Woodard, G.D. Cody, *Phys. Rev.* **136**, A166 (1964).

[23] E. Gratz, *J. Magn. Magn. Mater.* **29**, 181 (1982).

[24] N.F. Mott, H. Jones, *The Theory of the Properties of Metals and Alloys*, Oxford University Press, 1958.

[25] J.H. Mooij, *Phys. Status Solidi* **A17**, 521 (1973).